

Mathematical Modeling of Appendicular Bone Growth in Glaucous-winged Gulls

James L. Hayward,^{1*} Shandelle M. Henson,² John C. Banks,³ and Sheena L. Lyn²

¹Biology Department, Andrews University, Berrien Springs, Michigan 49104

²Department of Mathematics, Andrews University, Berrien Springs, Michigan 49104

³Physical Therapy Department, Andrews University, Berrien Springs, Michigan 49104

ABSTRACT Development of locomotor activity is crucial in tetrapods. In birds, this development leads to different functions for hindlimbs and forelimbs. The emergence of walking and flying as very different complex behavior patterns only weeks after hatching provides an interesting case study in animal development. We measured the diaphyseal lengths and midshaft diameters of three wing bones (humerus, ulna, and carpometacarpus) and three leg bones (femur, tibiotarsus, and tarsometatarsus) of 79 juvenile (ages 0–42 days) and 13 adult glaucous-winged gulls (*Larus glaucescens*), a semiprecocial species. From a suite of nine alternative mathematical models, we used information-theoretic criteria to determine the best model(s) for length and diameter of each bone as a function of age; that is, we determined the model(s) that obtained the best tradeoff between the minimized sum of squared residuals and the number of parameters used to fit the model. The Janoschek and Holling III models best described bone growth, with at least one of these models yielding an $R^2 \geq 0.94$ for every dimension except tarsometatarsus diameter ($R^2 = 0.87$). We used the best growth models to construct accurate allometric comparisons of the bones. Early maximal absolute growth rates characterize the humerus, femur, and tarsometatarsus, bones that assume adult-type support functions relatively early during juvenile development. Leg bone lengths exhibit more rapid but less sustained relative growth than wing bone lengths. Wing bone diameters are initially smaller than leg bone diameters, although this relationship is reversed by fledging. Wing bones and the femur approach adult length by fledging but continue to increase in diameter past fledging; the tibiotarsus and tarsometatarsus approach both adult length and diameter by fledging. In short, the pattern of bone growth in this semiprecocial species reflects the changing behavioral needs of the developing organism. *J. Morphol.* 000:000–000, 2008. © 2008 Wiley-Liss, Inc.

KEY WORDS: allometry; glaucous-winged gull; *Larus glaucescens*; bone growth; mathematical models

Locomotion in tetrapods is crucial for foraging, behavioral thermoregulation, and escape from predation. Newly born or hatched individuals, however, have small and weak limbs that must quickly develop appropriate properties. For birds this problem is particularly acute because the hindlimbs and forelimbs develop very different locomotor capabilities. A comparison of the respective

growth patterns of forelimbs and hindlimbs in birds clarifies the intricate and ever-changing balance maintained between limb growth and the locomotor capabilities in these animals (Carrier and Leon, 1990).

Gulls (family Laridae) constitute a group of semiprecocial birds that are strong walkers and agile fliers. Numerous data sets of externally measured size and growth features have been collected on gulls (Smith and Diem, 1972; Elowe and Payne, 1979; Dunn and Brisbin, 1980; Gilliland and Ankney, 1992), but little information is available on skeletal growth and allometry. Exceptions include Dinnendahl and Kramer (1957) and Klíma (1965), who examined skeletal relations by comparing dimensions of individual bones against the summed lengths of groups of bones in black-headed gulls (*Larus ridibundus*), herring gulls (*L. argentatus*), and great black-backed gulls (*L. marinus*); and Carrier and Leon (1990), who addressed the relationship of skeletal growth to bone strength, elasticity, and function in California gulls (*L. californicus*).

Here, we use rigorous mathematical modeling techniques to characterize the growth of six bones of the wing and leg in glaucous-winged gulls (*Larus glaucescens*) and discuss the interaction between skeletal and behavioral development in these birds. Because the functions of bones vary, one should not assume that a single model form is capable of predicting the growth of multiple bone types. In this study, we use an information-theoretic approach to determine the best model(s) from a suite of nine alternatives. By “best” we mean the model(s) that obtain the best tradeoff between the

Contract grant sponsor: Andrews University Faculty Grants; Contract grant sponsor: National Science Foundation; Contract grant numbers: DMS 0314512, DMS 0613899.

*Correspondence to: James L. Hayward, Biology Department, Andrews University, Berrien Springs, MI 49104.
E-mail: hayward@andrews.edu

Published online in
Wiley InterScience (www.interscience.wiley.com)
DOI: 10.1002/jmor.10669

minimized sum of squared residuals and the number of parameters used to fit the model. In addition, we demonstrate that most allometric relationships among long bone dimensions in this species are best determined by use of an allometric model based on the best growth models for the individual bones.

BEHAVIOR DEVELOPMENT

Before considering bone growth, for context we provide an overview of behavior development in glaucous-winged gulls. We divide development into seven stages: embryo, hatchling, early chick, late chick, fledgling, juvenile, and adult. Our study includes data from all but the embryo stage. Young glaucous-winged gulls are semiprecocial: they hatch fully feathered with open eyes and can walk within 1 day, but until fledging they must be parent-fed (James-Veitch and Booth, 1954; Hayward and Verbeek, 2008). The general sequence and timing of behavior development is summarized below from several sources (Schultz, 1951, 1986; James-Veitch and Booth, 1954; Vermeer, 1963; unpublished observations). Means and ranges are from Vermeer (1963); age in days is from day of hatching, day 0.

Embryo Stage (–27 to 0 Days)

During the 27 days (range = 25–30 days) between egg laying and hatching, all major organ systems develop. During the 3 days (range 1–5 days) at the end of this stage, the chicks pip and hatch.

Hatchling Stage (0–1 Day)

Wet down feathers dry 4–6 h after hatching. Fatigued hatchlings remain in the nest cup brooded by the parents. Hatchlings vocalize with a high-pitched call.

Early Chick Stage (2–14 Days)

Chicks move out of the nest, hide in grass, under logs, or under adults during most of this time. They peck at objects on the ground and beg for food. By the end of their first week, chicks may begin to jump up and down and flap their wings.

Late Chick Stage (15–43 Days)

Chicks at this stage are quite mobile. Toward the end of this stage they move in groups of like-aged birds that range outside their natal territories. Commonly, 5- to 7-week-old birds chase adult intruders out of territories. Older chicks jump and flap their wings progressively more vigorously, especially during the week before fledging.

Fledgling Stage (44–56 Days)

First flight occurs between 37 and 53 days (mean = 43.8 days, $n = 67$). As time progresses, fledglings circle above their territories and gain flight experience.

Juvenile Stage (57 Days to 4 Years)

Young gulls depart the colony for first time to feed between 48 and 67 days (mean = 55.6 days, $n = 135$). Juveniles, like adults, experience a complete molt each fall and partial molt each spring. Plumage becomes lighter each year until adulthood. First-year juveniles are initially weak and clumsy but gain strength and agility over time.

Adult Stage (4 Years to Death)

Adult glaucous-winged gulls are strong walkers, swimmers, and fliers. They forage over wide areas. Adult gulls set up and defend territories, form and maintain pair bonds, copulate, and defend their eggs and chicks from predators. Individuals that reach adulthood live an average of 13.5 years.

MATERIALS AND METHODS

Specimens Collected, Prepared, and Measured

From June to August 1989 and 1992, 373 newly-hatched, glaucous-winged gull, *Larus glaucescens*, chicks were banded on Violet Point, Protection Island National Wildlife Refuge (48°7'N, 122°55'W), Strait of Juan de Fuca, Washington. Each chick from a nest was designated as A, B, or C, depending on its position in the hatching sequence. The bodies of 125 of these known-aged (0–42 days) chicks and those of 13 adults (of unknown age), having died from natural causes, were retrieved and temporarily placed in a dermestid beetle (*Dermestes* sp.) box. At the end of the field seasons the partially cleaned skeletons were transported to the laboratory and frozen until preparation.

Thawed specimens were soaked for 7–10 days in 7% ammonium hydroxide, followed by maceration over a 2 to 3 h period in a pancreatin/sodium hydroxide solution. Cleaned, disarticulated skeletons were bleached overnight in a solution of 5% hydrogen peroxide then allowed to dry. At the completion of this process, 79 complete juvenile and 13 adult skeletons were obtained.

Diaphyseal length was measured from growth line to growth line of humeri, ulnae, carpometacarpi, femura, tibiotarsae, and tarsometatarsae, bones involved most directly in flying and walking. During skeletal development the epiphyses are not firmly attached to the diaphysis until age 9–10 days; thus we did not include epiphyses in any measurements. Midshaft diameter was measured along the widest axis. Age-stratified random sampling was used to create two sets of juvenile skeletons, one used for parameter estimation (“estimation data”) and the other used for an independent evaluation of the parameterized model (“validation data”).

Alternative Deterministic Growth Models Posed

We posed nine alternative models to describe the deterministic trends in bone growth. In each model below, $f(t)$ is the pre-

dicted bone size (length or diameter) in a chick of age t , and K , a , b , c , > 0 are parameters to be estimated from data. K is the asymptotic (adult) bone size, but a , b , c have various interpretations according to the model.

Holling Type I model. In the Holling Type I model bone growth is linear with age until a threshold age b at which growth stops at a maximal value K . This type of growth function was described by Holling (1959)

$$f_1(t) = \begin{cases} a(t-b) + K & \text{if } t < b \\ K & \text{if } t \geq b \end{cases} \quad (1)$$

The initial bone size (at age $t = 0$) is $K - ab$.

Holling Type III model. In the Holling Type III model (Holling, 1959) bones grow according to a sigmoidal (s-shaped) curve

$$f_2(t) = \frac{(K-b)t^2}{(a^2+t^2)} + b \quad (2)$$

The inflection point occurs at age $t = a/\sqrt{3}$. That is, for ages less than $a/\sqrt{3}$ the growth rate is increasing, and for ages greater than $a/\sqrt{3}$ the growth rate is decreasing. The initial size is b , and the (asymptotic) saturation size is K .

Modified Holling Type III model. This model is similar to model (2), except that the maximal size K is attained in finite time, at age c

$$f_3(t) = \begin{cases} \frac{(K-b)(a^2+c^2)t^2}{(a^2+t^2)c^2} + b & \text{if } t < c \\ K & \text{if } t \geq c \end{cases} \quad (3)$$

The initial size is b , and the inflection point occurs at age $t = a/\sqrt{3}$, provided $a/\sqrt{3} < c$. If $a/\sqrt{3} \geq c$, however, there is no inflection point.

Logistic model. The fourth model is sigmoidal with (asymptotic) saturation size K

$$f_4(t) = \frac{K}{1+ae^{-bt}} \quad (4)$$

The initial size is $K/(1+a)$, and the inflection point occurs at age $t = (\ln a)/b$.

Modified logistic model. This model is similar to model (4), except that the maximal size K is attained in finite time, at age c

$$f_5(t) = \begin{cases} \frac{K(1+ae^{-bc})}{(1+ae^{-bt})} & \text{if } t < c \\ K & \text{if } t \geq c \end{cases} \quad (5)$$

The inflection point occurs at age $t = (\ln a)/b$, provided $(\ln a)/b < c$; otherwise there is no inflection point. The initial size is $K(1+ae^{-bc})/(1+a)$.

Gompertz model. The Gompertz model (Gompertz, 1825) is sigmoidal with (asymptotic) saturation size K

$$f_6(t) = K \exp(-e^{a-bt}) \quad (6)$$

The initial size is $K \exp(-\exp(a))$, and the inflection point occurs at age $t = a/b$.

Modified Gompertz model. This model is similar to model (6), except that the maximal size K is attained in finite time, at age c

$$f_7(t) = \begin{cases} K \exp(e^{a-bc}) \exp(-e^{a-bt}) & \text{if } t < c \\ K & \text{if } t \geq c \end{cases} \quad (7)$$

The inflection point occurs at age $t = a/b$, provided $a/b < c$; otherwise there is no inflection point. The initial size is $K \exp(\exp(a-bc) - \exp(a))$.

Janoschek model. The Janoschek curve (Janoschek, 1957) is sigmoidal with (asymptotic) saturation size K , initial size a , and inflection point $t = ((c-1)/(bc))^{1/c}$:

$$f_8(t) = K - (K-a) \exp(-bt^c) \quad (8)$$

Modified Janoschek model. This model is similar to model (8), except that the maximal size K is attained in finite time, at age c

$$f_9(t) = \begin{cases} K + K \exp(-ac^b) - K \exp(-at^b) & \text{if } t < c \\ K & \text{if } t \geq c \end{cases} \quad (9)$$

The inflection point occurs at age $t = ((b-1)/(ab))^{1/b}$, provided $((b-1)/(ab))^{1/b} < c$; otherwise there is no inflection point. The initial size is $K \exp(-ac^b)$.

Stochastic Model Specified

To connect Eqs. 1–9 to data, one must model the departures of data from predictions, that is, one must model the distribution of residuals. This is done by specifying a stochastic model. A useful approach is that of the “deterministic skeleton plus noise,” in which observations are modeled as the deterministic prediction (the “trend”) plus an error term that is normally distributed with constant variance. Typically, however, data and predictions must be transformed (for example by a logarithm or square root) in order for the distribution of residual errors to satisfy normality and homoskedasticity (constant variance) assumptions (Henson et al., 2007).

Motivated by a post-hoc inspection of histograms and QQ-plots of fitted residuals obtained under logarithmic, square root, and identity transformations, we chose the natural logarithm as the variance-stabilizing transformation. That is, we used the stochastic model

$$\ln(Y(t)) = \ln(f(t)) + \sigma_J E, \quad (10)$$

where t is the age of the chick in days, the random variable Y denotes bone length or diameter at age t , the value $f(t)$ is the deterministic prediction for the bone length or diameter at age t , the random variable E is standard normal (mean zero and standard deviation one), and $\sigma_J \geq 0$ is a constant that is independent of age and bone size. Equation 10 implies that the hypothesized distribution of the residuals of the log-transformed data and predictions is normal with mean zero and standard deviation σ_J .

The stochastic model (10) can be simplified algebraically as

$$Y(t) = f(t) \exp(\sigma_J E). \quad (11)$$

Model Parameters Estimated

Each deterministic skeleton $f(t)$ contains three parameters (a , b , K) or else four parameters (a , b , c , K), and the stochastic version of each model contains an additional parameter σ_J .

Because the ages of the dead adults were unknown, the adult data could not be included in the estimation data set used for least squares model-fitting. Thus, the parameter K was estimated directly from the adult data, which were assumed to be lognormally distributed. By Shimizu and Iwase (1981) and Dennis et al. (1991), a uniformly minimum variance unbiased (UMVU) estimator of the mean of the lognormal distribution is

$$K = \exp(\hat{\mu}_A)_0 F_1 \left(\frac{q-1}{2}; \frac{q-1}{4} \hat{\sigma}_A^2 \right), \quad (12)$$

where $\hat{\mu}_A$ and $\hat{\sigma}_A^2$ are the sample mean and variance of the log-transformed adult data, q is the sample size, and ${}_0F_1(v; z)$ is the hypergeometric series

TABLE 1. Best growth models for length and diameter of each of six appendicular bones in *Larus glaucescens*, with LS estimates for parameters a , b , and c

Bone	Model (#)[Not Inferior]	S_0 (cm)	Age (days)	G (cm/day)	K (cm)	a_{EST}	b_{EST}	c_{EST}	R^2_{EST}	R^2_{VAL}
Humerus										
Length	Mod Jan (9) [1,4,5,7,8]	2.787	13.2	0.2796	11.97	0.007629	1.413	41.21	0.99	0.98
Diam	Jan (8) [6,7,9]	0.1226	7.0	0.01613	0.7324	0.1226	0.01676	1.224	0.98	0.96
Ulna										
Length	Jan (8) [3,9]	1.467	22.0	0.4390	13.95	1.467	0.0003763	2.376	0.99	0.98
Diam	Holl III (2) [3,8,9]	0.09610	12.7	0.01677	0.6632	21.97	0.09610	N/A	0.97	0.95
Carpometacarpus										
Length	Jan (8) [3,9]	0.8183	22.4	0.2249	6.916	0.8183	0.0002477	2.507	0.98	0.96
Diam	Holl III (2) [3,4,8,9]	0.07362	14.2	0.01131	0.5031	24.66	0.07362	N/A	0.96	0.95
Femur										
Length	Holl III (2) [3,4,5,8]	1.581	7.4	0.2168	5.847	12.78	1.581	N/A	0.98	0.98
Diam	Holl III (2) [3,4,8]	0.1864	7.0	0.01730	0.5108	12.18	0.1864	N/A	0.97	0.96
Tibiotarsus										
Length	Jan (8) [3,5,9]	1.484	16.7	0.3827	10.79	1.484	0.001178	2.178	0.98	0.98
Diam	Jan (8) [1,3,5,7,9]	0.1980	11.4	0.01813	0.5163	0.1980	0.003215	2.093	0.96	0.94
Tarsometatarsus										
Length	Mod Holl III (3) [2,4,5,8,9]	1.709	10.7	0.1866	6.501	18.48	1.709	56.27	0.98	0.97
Diam	Mod Jan (9) [1,3,8]	0.2321	13.7	0.01347	0.4239	0.005361	1.641	17.78	0.93	0.85

Arbitrarily, only the values for models with $\Delta AIC = 0$ (parentheses) are tabulated, although models with $\Delta AIC \leq 10$ [brackets] cannot be considered inferior. Initial size (S_0), age at maximal absolute growth rate (Age), and maximal absolute growth rate (G) were computed from the LS parameters and the formulas given in the text near equations (1)–(9). Maximal bone dimension (K) was estimated from the adult data using equation (12). R^2 values are shown for estimation (R^2_{EST}) and validation (R^2_{VAL}) data sets.

$${}_0F_1(v; z) = \sum_{j=0}^{\infty} \left(\frac{z^j}{j! \prod_{k=0}^{j-1} (v+k)} \right) = 1 + \frac{z}{v} + \frac{z^2}{2v(v+1)} + \frac{z^3}{3v(v+1)(v+2)} + \dots \quad (13)$$

The infinite series is truncated once the desired accuracy has been reached. The estimated value of K for each bone is listed in Table 1.

Values of the remaining parameters in the deterministic skeleton were estimated from the estimation data set by the method of nonlinear least squares (LS). That is, we minimized the residual sum of squares

$$RSS(\theta) = \sum_{\text{data}} (\ln(\text{observation}) - \ln(\text{prediction}))^2 \quad (14)$$

as a function of the vector θ of model parameters. The minimizer $\hat{\theta}$ is the vector of LS parameter estimates for the model. We used MatLab to minimize $RSS(\theta)$ with the Nelder-Mead downhill method (Olsson and Nelson, 1975; Press et al., 1986).

The value of $\hat{\sigma}_j^2$ is estimated from the fitted residuals by

$$\hat{\sigma}_j^2 = RSS(\hat{\theta})/n, \quad (15)$$

where n is the number of observations (Burnham and Anderson, 2002, p. 63).

Best Models Selected

We used the Akaike Information Criterion (AIC; Burnham and Anderson, 2002), an information-theoretic model selection index designed to select the best model from a suite of alternatives (Peck et al., 2002). For the LS method the criterion is equivalent to

$$AIC = n \ln \hat{\sigma}_j^2 + 2\kappa \quad (16)$$

where n is the number of observations and κ is the number of estimated model parameters, including σ_j . The actual value of AIC, which can be positive or negative, does not give any infor-

mation. Rather, model comparison is based on the rank of the AIC values for the suite of alternative models. The smallest value AIC_{\min} indicates the best model. For each model we computed $\Delta AIC = AIC - AIC_{\min}$. Burnham and Anderson (2002, p. 70) provide the following “rule of thumb” for nested models: Models with $\Delta AIC > 10$ have essentially no level of empirical support for approximating the given data and can be discarded. They also note that the cutoff may be somewhat higher for non-nested models, and that this is an area of ongoing research. Although our set of alternative models is not nested, we arbitrarily follow the cutoff value of $\Delta AIC = 10$ in this study.

Models Validated

We tested the best models on the validation data set without reparameterizing. That is, for each model with $\Delta AIC \leq 10$, we compared the (fitted) goodness-of-fit on the estimation data set to the goodness-of-fit on the validation data set without re-estimating parameters for the latter data. We computed the goodness-of-fit with a generalized R^2 given by

$$R^2 = 1 - \frac{\sum_{\text{data}} (\ln(\text{observation}) - \ln(\text{prediction}))^2}{\sum_{\text{data}} (\ln(\text{observation}) - \text{mean}(\ln(\text{observation})))^2}, \quad (17)$$

where “mean” denotes the sample mean of the log-transformed data. The value of R^2 represents the proportion of the observed variability that is explained by the model, and thus gives a measure of the accuracy of model predictions.

Absolute and Relative Growth Rates Determined

From the best-fit model for each bone dimension, we determined both absolute and relative growth rates. An absolute growth rate indicates the actual rate of growth in cm/day at a given moment, and is given by the first derivative df/dt of the growth function $f(t)$. Absolute growth rates are most useful for interpretation of within-bone growth. If all bones had the same initial dimensions and grew to the same final dimensions, their absolute rates of growth could be compared directly. Given this

is not the case, relative growth rates provide more reasonable between-bone growth comparisons. A relative growth rate is determined by dividing the absolute growth rate by the current size of the bone, that is $(df/dt)/f(t)$. The relative growth rate is the growth rate per cm of bone, and has units of cm/day/cm, that is, 1/day. Thus, if two bones have the same absolute growth rate, then the longer bone has the smaller relative growth rate; and if two bones have the same relative growth rate, then the longer bone has the larger absolute growth rate. The area under the relative growth rate curve between age 0 and age τ represents the relative length (or diameter) of the bone at age τ , and is given by

$$\int_0^{\tau} \frac{1}{f(t)} \frac{df}{dt} dt = \ln f(t)|_0^{\tau} = \ln f(\tau) - \ln f(0) = \ln \frac{f(\tau)}{f(0)}. \quad (18)$$

That is, we take the current relative size of the bone to be the natural logarithm of the ratio of the current size to the initial size.

Allometric Model Developed and Trends Assessed

For the allometric analysis, both estimation and validation data were used for parameter estimation. We posed two alternative types of allometric models.

In the “standard” allometric model, two body measurements x and y taken at age t are related by the equation

$$y = ax^b, \quad (19)$$

that is,

$$y(t) = a(x(t))^b, \quad (20)$$

where a and b are parameters to be determined from data. We used the stochastic model

$$\ln(Y) = \ln(aX^b) + \sigma E \quad (21)$$

where E is a standard normal random variable, $\sigma \geq 0$ is constant, and X and Y are random variables denoting the bone measurements.

An “alternate” allometric model was constructed directly from the best growth models for the body measurements x and y . Suppose $x(t) = f_i(t)$ and $y(t) = f_j(t)$ are the best growth models for body dimensions x and y , where f_i and f_j denote models from the suite of alternatives listed in (1)–(9). Each f_i is an increasing function of t , and is hence invertible, so we can solve for age t as a function of size x by $t = f_i^{-1}(x(t))$. Substituting this expression into the right hand side of equation $y(t) = f_j(t)$ yields a relationship between x and y via the model

$$y(t) = f_j(f_i^{-1}(x(t))). \quad (22)$$

Note that model (22) does not require parameterization, since the LS parameters were already computed for the growth models.

Growth of A/B and C Chicks Compared

To test whether bones of C chicks exhibited growth patterns different from bones of A and B chicks (Parsons, 1975; Salzer and Larkin, 1990), we fitted the models to the A/B chick data and then used the models to predict the C chick data without refitting. In particular, for each bone dimension we re-estimated parameters for the previously determined best model (the one with $\Delta AIC = 0$) using the A/B data. Then, without re-estimat-

ing parameters, we computed the goodness-of-fit on the C data and compared it to the goodness-of-fit on the A/B data.

RESULTS

Absolute Growth

The best growth models for length and diameter of each bone, with model parameter values and R^2 values for estimation and validation data sets, are indicated in Table 1. Only values for models for which $\Delta AIC = 0$ are tabulated, although models with $\Delta AIC \leq 10$ are not considered inferior and are listed in square brackets. (All model parameters, ΔAIC , and R^2 values are available upon request.) For lengths and diameters of all six bones, the best models ($\Delta AIC = 0$) are always the Holling III or Janoschek models, in either their basic or modified forms. For each of the twelve dimensions, however, between two and five models are not discarded because $\Delta AIC \leq 10$. Moreover, each of the nine models appears at least once in the square bracket lists of suitable models. All R^2 values for models with $\Delta AIC \leq 10$ are >0.90 , except for tarsometatarsal diameter validation R^2 values, which range between 0.83 and 0.87.

The predictions of the best model ($\Delta AIC = 0$) for each bone dimension are shown with the data in Figures 1 and 2. Note that the shape of the modified Janoschek model curve for tarsometatarsus diameter appears atypical because growth termination is predicted to occur quite early, at 17.78 days (Fig. 2C). A series of diagrams that illustrates the predicted change in absolute length and diameter of each bone from hatchling to adult stages is shown in Figure 3.

Maximum Absolute Growth Rates

Maximal absolute growth rates (arrows, Figs. 1, 2) for length are predicted to occur later for the proximal-to-distal sequence of wing bones (see Fig. 1) than for the corresponding proximal-to-distal sequence of leg bones (see Fig. 2). In contrast, maximal absolute growth rates for diameters of the proximal-to-distal sequences of both of wing and leg bones are predicted to occur close to the same time. For both length and diameter, maximal absolute growth rates for the humerus and femur are predicted to occur earlier than for the other bones of the wing and leg, respectively (Figs. 1A, 2A).

Relative Growth

Relative growth curves, computed as the natural logarithm of the ratio of the predicted bone size to the predicted initial size (see Eq. 18), are shown in Figure 4. The humerus is predicted to be relatively longer than the ulna and carpometacarpus until days 10–13, at which time this relationship is

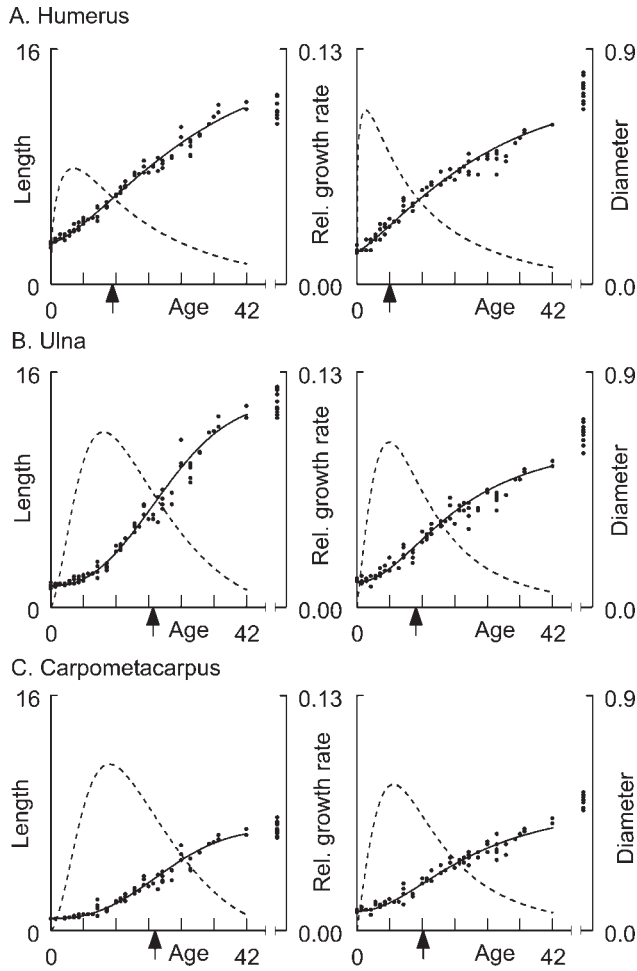


Fig. 1. Growth in length and diameter of the humerus, ulna, and carpometacarpus by age (days) in *Larus glaucescens*. In each graph the solid line depicts the best-fit growth model from Table 1, and the dotted line depicts the relative growth rate (see Methods) for that bone. The arrows mark the age of maximal absolute growth rate which occurs at the inflection point of the growth curve. The adult data appear in the far right of each plot window. All dimensions in cm.

reversed (Fig. 4A). Moreover, relative growth curves of the ulna and carpometacarpus are predicted to closely resemble one another. A similar relative growth pattern is predicted for wing bone diameters, although the cross-over time is later (Fig. 4C). Among the leg bones, the femur is predicted to be relatively longer during the first week and a half, at which time the tibiotarsus takes the lead (Fig. 4B). The diameter of the femur is predicted to be relatively larger than that of the tibiotarsus during the first two and one half weeks (Fig. 4D).

The femur is predicted to approach relative maximum length before the tarsometatarsus, although relative growth curves for the two bones resemble one another (Fig. 4B). In contrast, the tarsometatarsus diameter is predicted to stop growing at

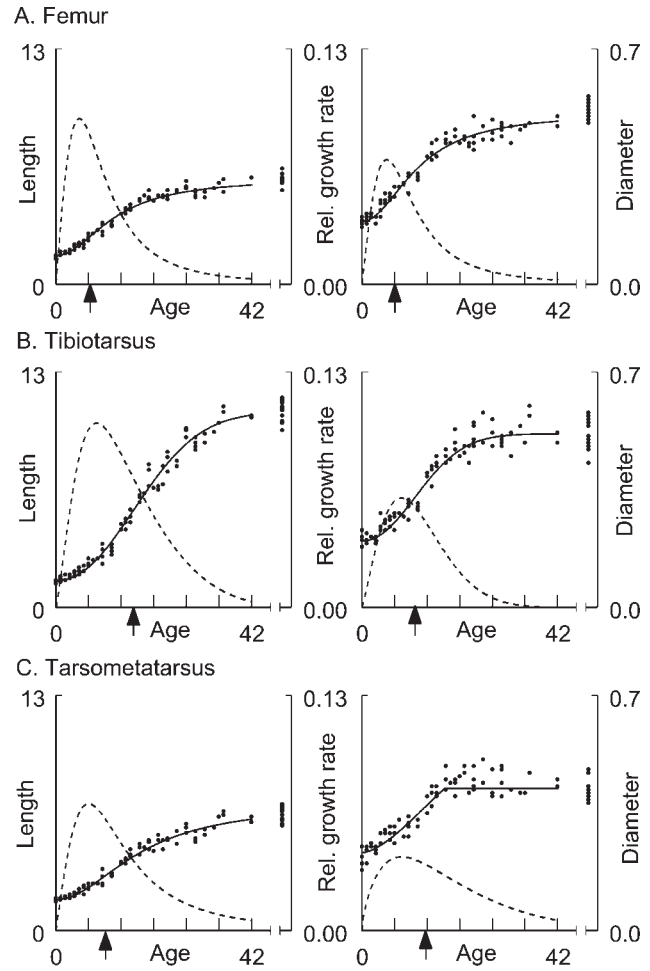


Fig. 2. Growth in length and diameter of the femur, tibiotarsus, and tarsometatarsus by age (days) in *Larus glaucescens*. See Figure 1 for details on how to interpret each graph.

about 18 days, while the femur diameter continues to grow (Fig. 4D).

The relative growth of the humerus diameter always exceeds that of length (Fig. 4E). Relative growth of the ulna and carpometacarpus diameter is predicted to exceed that of the length until day 16, when the situation is reversed (Fig. 4G,I). For the leg bones, relative growth in length exceeds relative growth in diameter throughout pre-fledging development (Fig. 4F,H,J).

During postnatal development, the tibiotarsus is predicted to grow to approximately seven times its natal length (Table 1; compare K and S_0), whereas the femur, tarsometatarsus, and humerus grow to only about four times their initial lengths. The ulna and carpometacarpus grow to about nine times their natal lengths. Thus, the leg experiences less postnatal growth than the wing. An inspection of the K values in Table 1 shows that the femur makes relatively less contribution (25%) to final leg length than does the humerus (36%) to

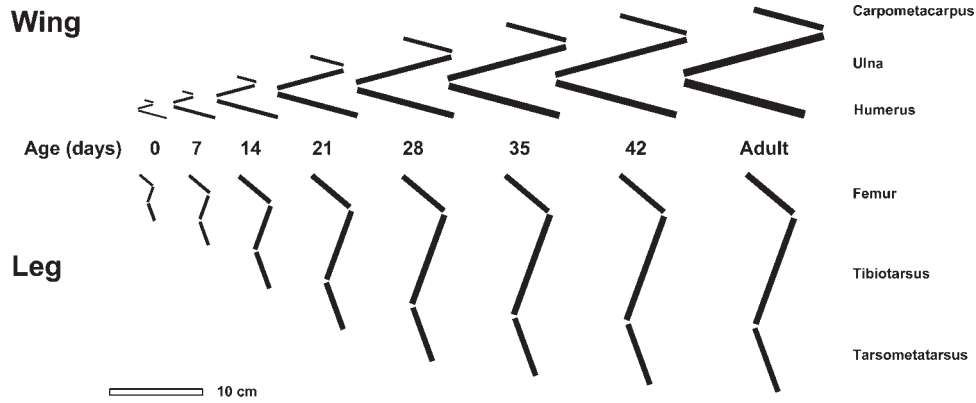


Fig. 3. A series of diagrams that illustrate predicted changes in absolute length and diameter of each of three articulated long bones of the wing and three articulated long bones of the leg in *Larus glaucescens*. Bones are drawn to scale; length is from growth line to growth line (minus epiphyses) and diameter is of the midshaft.

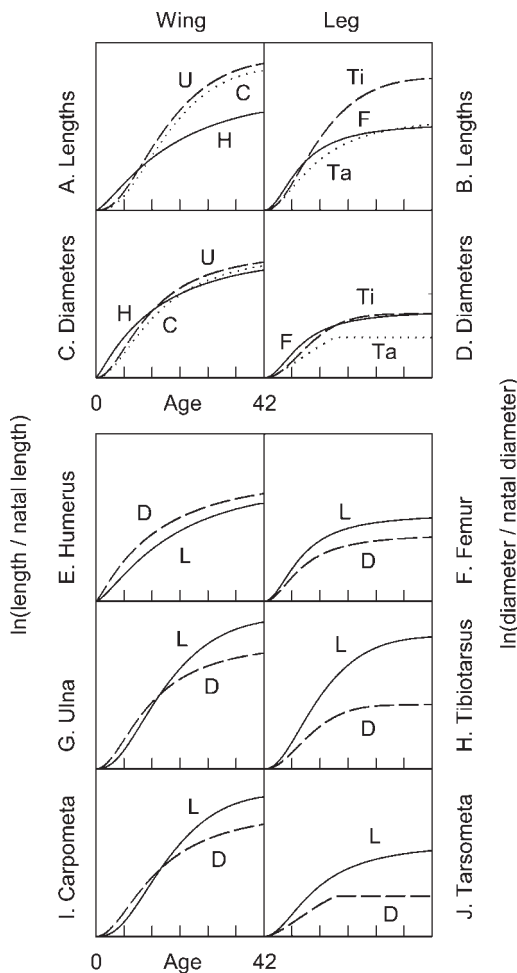


Fig. 4. Comparisons among predicted relative growth curves for selected bone dimensions in *Larus glaucescens*. Each vertical axis ranges from 0 to 2.5. The following bone abbreviations are used in plot windows A–D. C, carpometacarpus; F, femur; H, humerus; Ta, tarsometatarsus; Ti, tibiotarsus; U, ulna. In plot windows E–J, solid lines (L) represent lengths and dashed lines (D) represent diameters.

final wing length. A comparison of juvenile growth predictions/data and adult data in Figures 1 and 2 shows that the bones of the wing, as well as the femur, approach adult length by fledging but continue to increase in diameter past fledging. In contrast, the tibiotarsus and tarsometatarsus approach both adult length and adult diameter by fledging.

Allometric Models

The goodness-of-fits of the standard and alternate allometric models (models 20 and 22, respectively) are compared in Table 2. Model (22) yields higher R^2 values except in the case of the humeral diameter vs. the femoral diameter, in which case model (20) fits better.

Allometric model predictions and data are shown together in Figures 5–7. Allometric growth patterns are similar for both length and diameter comparisons (Figs. 5, 6). Early in development, growth of humeral length and diameter is more rapid than that of the ulna and carpometacarpus (Figs. 5A,B, 6A,B). Concave-up allometric curves for humeral vs. femoral lengths and diameters show that femoral growth slows long before the humerus terminates growth (Figs. 5C, 6C). The allometric relationship for the ulna versus carpometacarpus, both in length and diameter, is virtually linear (Figs. 5D, 6D). Ulnal and carpometacarpal diameters continue to grow after cessation of growth in tibiotarsus and tarsometatarsus diameters, respectively (Fig. 6H,I). Growth of tarsometatarsal diameter halts before this bone stops growing in length.

A/B and C Chick Comparison

Table 3 compares the A/B chick data to the C chick data for each bone dimension using the best

TABLE 2. LS parameters a and b for the standard allometric model $y = ax^b$, and R^2 values for standard (R^2_{STD}) and alternate (R^2_{ALT}) allometric models for bone growth in *Larus glaucescens*

Pairing	a_{STD}	b_{STD}	R^2_{STD}	R^2_{ALT}
Length vs. length (y vs. x)				
Humerus/Ulna	2.556	0.6057	0.97	0.98
Humerus/Carpometacarpus	3.843	0.6087	0.97	0.98
Humerus/Femur	1.709	1.008	0.95	0.97
Ulna/Carpometacarpus	1.913	1.025	0.99	0.99
Femur/Tibiotarsus	1.410	0.6186	0.95	0.98
Femur/Tarsometatarsus	1.013	0.9828	0.97	0.98
Tibiotarsus/Tarsometatarsus	0.6030	1.566	0.98	0.99
Tibiotarsus/Ulna	1.153	0.9930	0.98	0.99
Tarsometatarsus/Carpometacarpus	2.280	0.5871	0.94	0.98
Diameter vs. diameter				
Humerus/Ulna	1.022	0.8345	0.97	0.98
Humerus/Carpometacarpus	1.254	0.7946	0.92	0.94
Humerus/Femur	1.467	1.428	0.95	0.94*
Ulna/Carpometacarpus	1.3180	0.9752	0.94	0.95
Femur/Tibiotarsus	0.8378	0.8796	0.93	0.96
Femur/Tarsometatarsus	1.160	1.189	0.88	0.94
Tibiotarsus/Tarsometatarsus	1.432	1.347	0.91	0.95
Tibiotarsus/Ulna	0.8717	0.6321	0.94	0.95
Tarsometatarsus/Carpometacarpus	0.7114	0.3947	0.83	0.89
Length vs. diameter				
Femur	14.52	1.323	0.97	0.97
Tibiotarsus	29.43	1.868	0.95	0.97
Tarsometatarsus	18.17	1.594	0.88	0.92
Humerus	17.55	0.9272	0.95	0.98
Ulna	25.28	1.295	0.95	0.97
Carpometacarpus	19.51	1.296	0.97	0.98

The only comparison for which $R^2_{STD} > R^2_{ALT}$ is indicated with an asterisk (*).

models ($\Delta AIC = 0$) from Table 1. In all but one case, the validation (C chick) R^2 values are within 0.04 of the estimation (A/B) R^2 values. The exception is the tarsometatarsal diameter, in which case the validation R^2 decreases more than 0.04. To further investigate whether the tarsometatarsal diameter might grow differently in C as opposed to A/B chicks, we refitted models (1)–(9) to both the C and A/B data sets separately. The Holling I model (1) provides a best-fit model ($\Delta AIC \leq 10$) for both. Thus, the tarsometatarsal diameter does not grow according to different models for C as opposed to A/B chicks. The Holling I parameters were $a = 0.009785$, $b = 20.01$ for A/B chicks, and $a = 0.01184$, $b = 18.00$ for C chicks. That is, tarsometatarsal diameters for A/B chicks are predicted to stop growing at age 20 days, whereas the tarsometatarsal diameters for the C chicks are predicted to stop growing at age 18 days (see Fig. 8). In general, our data do not allow us to reject the null hypothesis that growth of appendicular long bones in A/B chicks is the same as those in C chicks.

DISCUSSION

The most reliable index of morphological development in birds is growth of the skeleton, a process little influenced by external factors (Klíma, 1965; Livezey and Storer, 1992). The appendicular skeleton of most tetrapods consists of four sets of

long bones within limbs, plus a variety of small bones that form the digits at the distal end of each limb. Each forelimb and hindlimb is composed of three main sections jointed to one another and jointed proximally to the axial skeleton at the pectoral and pelvic girdles, respectively. Attached skeletal muscles move the long bones relative to one another and relative to the axial skeleton to achieve locomotion. Our study is concerned with the ontogeny of bone size in each of the three main sections of the forelimb and of the hindlimb, respectively, in relation to the ontogeny of walking and flying in a semiprecocial species of bird.

Growth of long bone length is by endochondral ossification, which occurs just below the growth plate cartilage at each end of the diaphysis. Ossification occurs by calcification of a mineralized matrix constructed by chondrocytes, which die before the onset of ossification. Before death, the chondrocytes lengthen in the same direction as the long axis of the bone. This hypertrophy is responsible for most long bone lengthening, although pre-hypertrophy mitosis also plays a role. Growth of long bone diameter along the diaphysis is by calcification of the osteogenic layer of the periosteum (Hall, 2000).

A variety of factors interact to control bone growth. Bone growth mediators, including cytokines, growth factors, and hormones are responsible for local control of the process. Nutrition and

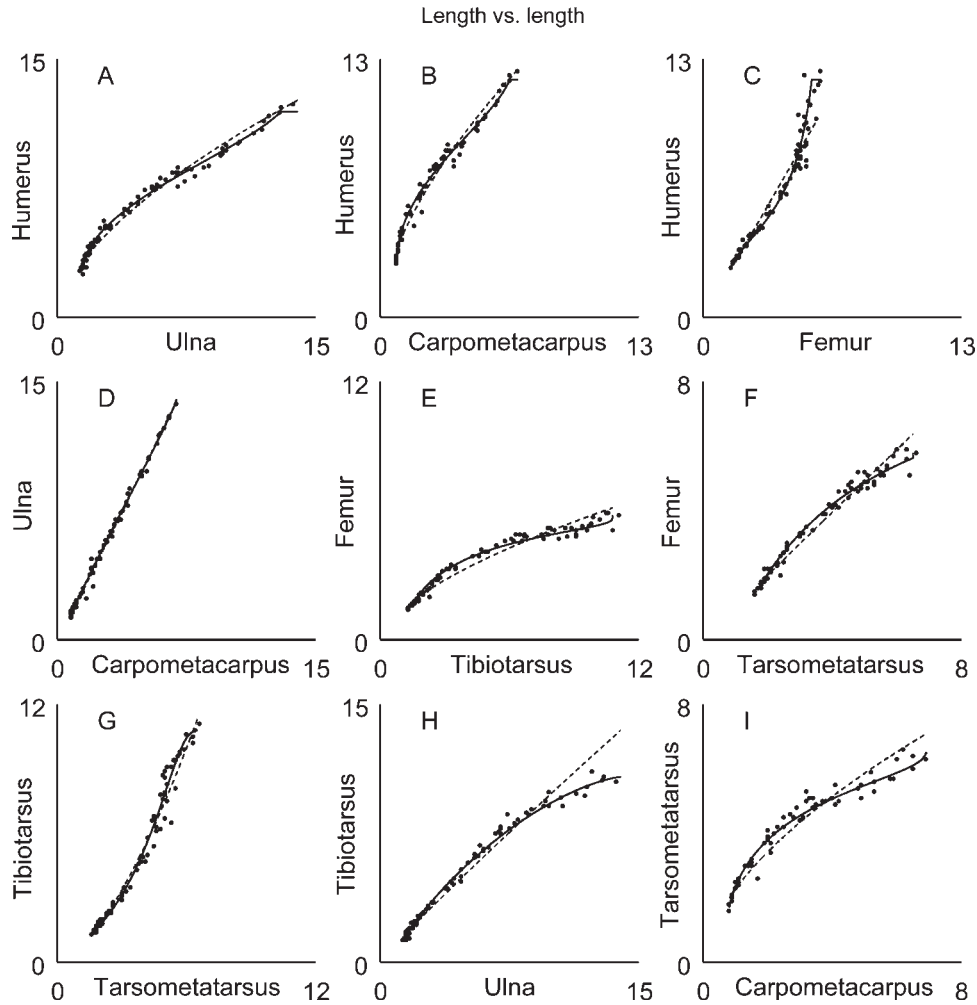


Fig. 5. Allometric relations for selected pairs of bone lengths in *Larus glaucescens*. In each graph the dotted line represents the best-fit model using the standard allometric formula $y = ax^b$ whereas the solid line represents the best-fit model constructed directly from the best growth models (see Methods).

mechanical stress also play important roles, and disease can alter growth. Thus, bone growth rates are determined by a complex suite of factors and interactions, many of which remain incompletely understood. Global control of the process is primarily genetic, whereas local control depends on the interaction and availability of growth mediators and nutrients (Price et al., 1994). Suffice it to say it is impossible to provide a completely satisfying mechanism for the growth and development of any particular bone. What can be done is to compare various rates of growth to understand how the developing organism differentially appropriates available nutrients and growth factors to various growth plates and periosteal changes in size that are functionally coordinated with ontogenetic changes in behavior.

The coordination of skeletal growth represents millions of generations of natural selection.

Growth rates for individual bones correspond with finely honed compromises among factors such as hatching-to-fledging time, changes in biomechanical stress, and the ontogeny of behavior. Adult gulls are strong walkers and agile fliers so successful development will lead to individuals finely tuned for both locomotory modalities. Thus it is not surprising that long-bone growth data show such little variability and match model predictions so well. Indeed, because of its relative uniformity within species, skeletal growth has been used in several studies of avian growth allometrics (Dinnendahl and Kramer, 1957; Meunier, 1959; Gille and Salomon, 1995, 1999; Gille et al., 2000).

The Janoschek model has been suggested as providing the best fit for growth data for body parts of many species (Gille and Salomon, 1995). Our results are consistent with this conclusion; this model, in its original (model 8) or modified form

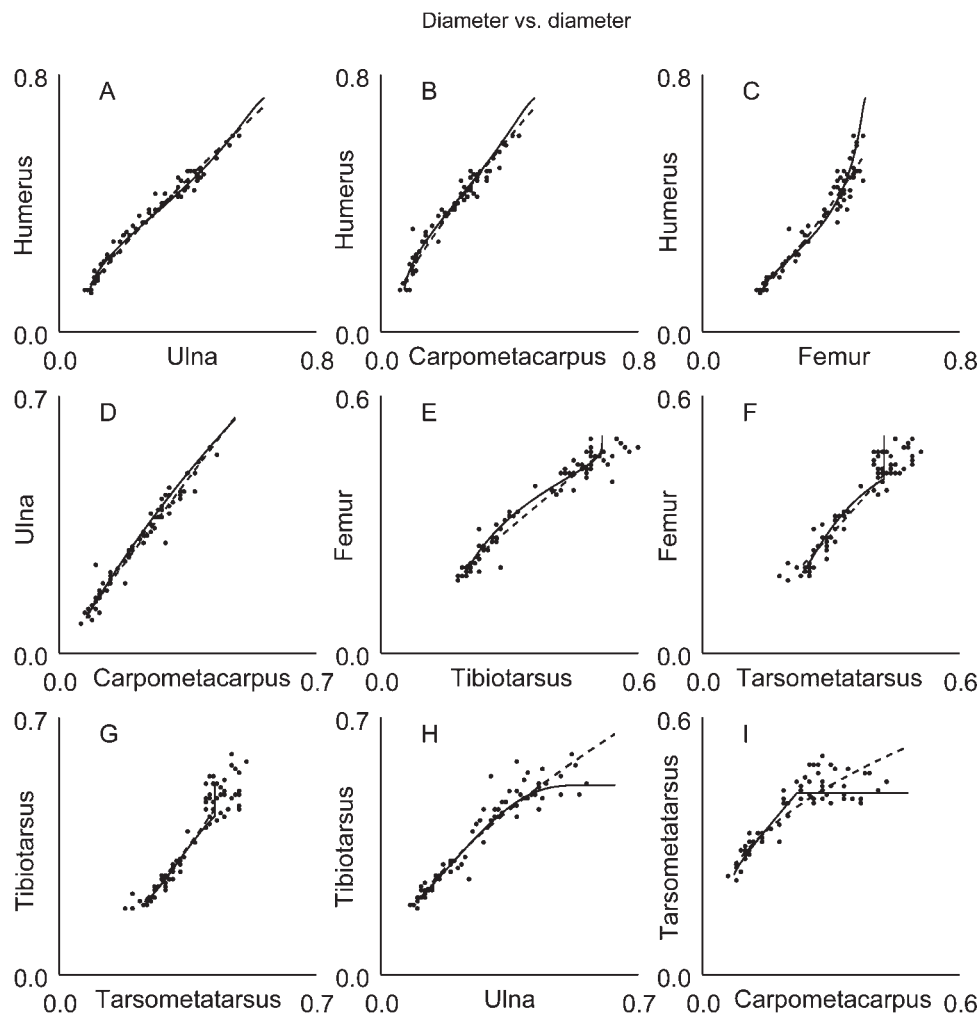


Fig. 6. Allometric relations for selected pairs of bone diameters in *Larus glaucescens*. See Figure 4 for details on how to interpret each graph.

(model 9), is among the best models for both the length and diameter for each of the six bones, the only model for which this is true. Both the Janoschek and Holling III models describe sigmoidal growth, which involves an initial phase of exponential increase in chondrocyte mitosis and/or hypertrophy (bone length) and periosteal growth and calcification (bone diameter), followed by a phase of diminishing growth that leads to growth termination. The maximal absolute growth rate occurs at a time that corresponds with the inflection point of the growth curve (arrows, Figs. 1,2).

The inflection point occurs early in growth of the humerus, which provides early support and muscle attachments for the rapidly elongating wing, and in growth of the femur and tarsometatarsus, which provide early terrestrial locomotory support for the semiprecocial juvenile. Conversely, this point occurs relatively later in growth of the ulna and carpometacarpus, to which are anchored the primary and secondary flight feathers, respectively,

that become functional only at fledging. In short, early maximal absolute growth rates characterize bones that assume adult-type behavioral functionality relatively early during juvenile development.

Relative differences in bone dimensions in differently sized organisms were discussed by Galileo in the seventeenth century (Galilei, 1638 [1914]). Relative growth curves of bone dimensions provide insight into growth in relation to initial size. This allows for a "fair" comparison between various bones. If all parts of a 1-day-old hatchling proceeded to grow at the same relative rate, an individual that was 44-days old, the average age at fledging, would retain the proportions it exhibited as a hatchling, although now it would be much larger, more awkward, and unable to fly. Comparisons among relative growth curves of body parts allow for an assessment of whole-body morphogenesis.

Most interesting in this regard is the relative growth of wing and leg bone lengths, respectively.

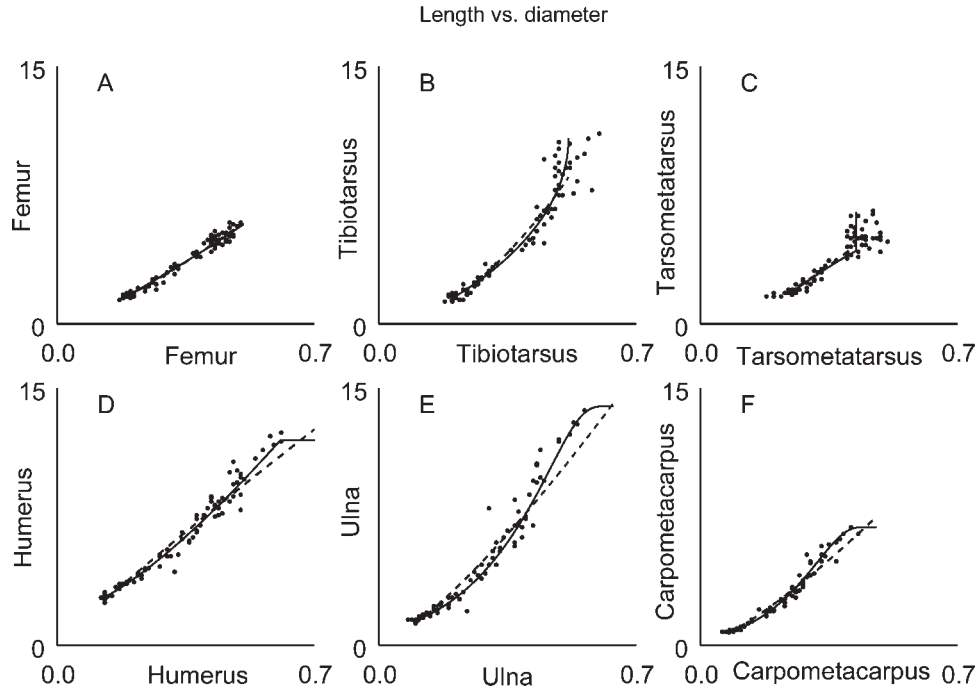


Fig. 7. Allometric relations for selected bone lengths with bone diameters in *Larus glaucescens*. See Figure 4 for details on how to interpret each graph.

TABLE 3. A/B chick data compared to C chick data for *Larus glaucescens* using the best models from Table 1

Bone	Best growth model (no.)	R^2_{EST}	R^2_{VAL}
Lengths			
Humerus	Mod Janoschek (9)	0.98	0.98
Ulna	Janoschek (8)	0.98	0.98
Carpometacarpus	Janoschek (8)	0.96	0.96
Femur	Holling III (2)	0.98	0.98
Tibiotarsus	Janoschek (8)	0.99	0.97
Tarsometatarsus	Mod. Holling III (3)	0.98	0.97
Diameters			
Humerus	Janoschek (8)	0.97	0.97
Ulna	Holling III (2)	0.95	0.97
Carpometacarpus	Holling III (2)	0.97	0.94
Femur	Holling III (2)	0.97	0.96
Tibiotarsus	Janoschek (8)	0.96	0.94
Tarsometatarsus	Mod Janoschek (9)	0.92	0.87*

A/B data were used as estimation data to parameterize the model (resulting in R^2_{EST}) and C data were used as validation data (resulting in R^2_{VAL}). The single validation R^2 value that differs from corresponding estimation R^2 values by more than 0.04 is indicated with an asterisk (*).

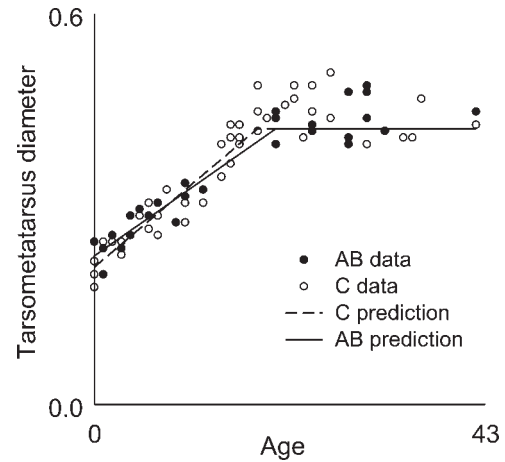


Fig. 8. Comparison between A/B and C chick tarsometatarsus diameters by age in *Larus glaucescens*. Note how little the data sets differ.

The hatchling humerus immediately functions to support the entire wing, which lies folded against the side of the body and attached to the body at a single point. Given this supportive function, as well as rapid growth of the nascent but all-important pectoralis (flight) muscle already attached to this bone, humeral growth dominates forelimb development for the first 2 weeks. Beginning in the third week and continuing on to fledging, however, relative growth of the ulna and carpometacarpus

exceeds that of the humerus. The ulna increases in length by over 900% from hatching to fledging, and the carpometacarpus increases by nearly the same percent.

A similar pattern is observed in the relative growth of the leg bones. Hatchling leg bone diameters are considerably greater than corresponding wing bone diameters. Moreover, relative growth of the leg bones exhibits a more rapid although less sustained rise in length than growth of the wing

bones. Chicks begin to walk within a day of hatching, whereas the first flight occurs about 6 weeks later; the two growth patterns thus reflect the differing locomotory ontogenies. Notably, both tibiotarsal and tarsometatarsal diameters achieve or nearly achieve adult size well before fledging, although they continue to grow in length.

Although wing bone diameters are initially smaller than leg bone diameters, this relationship is reversed by fledging (both absolutely and relatively) and adult wing diameters are considerably larger than adult leg diameters (K and S_0 , Table 1). Fledging diameters for all three forelimb bones are consistently lower than eventual adult diameters (see Fig. 1). Fledgling gulls are weak and relatively clumsy fliers; postfledging forelimb growth may in part be a response of bone tissue to increased mechanical stresses as flight becomes more powerful and agile (Carrier and Leon, 1990). By contrast, gulls appear to optimize their walking capabilities well before fledging. Thus, the pattern of bone growth follows the emerging behavioral needs of the growing organism.

The hypothesis that the rate of bone growth limits the minimum fledging time of birds was tested by Carrier and Auriemma (1992). Their examination of 25 families of birds showed a strong correlation between fledging period and wing bone length in relation to body mass. Thus, relatively short-winged birds fledge sooner than relatively long-winged birds. For example, short-winged ring-necked pheasants (*Phasianus colchicus*) are highly precocial and fledge at 11 days (Carrier and Auriemma, 1992; Montes et al., 2005). By contrast, long-winged glaucous-winged gulls of similar mass fledge at 44 days. The longer pre-fledging duration in gulls may be due in part to a need for more time to grow longer wings.

We did not evaluate breakage properties of bones in this study, although they constitute an important component of long bone function. In closely related California gulls, appendicular bone strength and stiffness increase by a factor of six to ten during post-hatching growth (Carrier and Leon, 1990). Moreover, the relatively thick hindlimbs of juveniles compensate for their relatively weak tissue, whereas forelimbs remain thin and weak for most of the pre-fledging period, a reflection of the early importance of walking. Once juveniles begin to exercise their wings, however, breaking loads for wing bones greatly increase, a trend paralleling a greatly increased surface area of the wing and pectoralis muscle mass. Results for California gulls and those reported here for glaucous-winged gulls support the conclusion that larid forelimbs and hindlimbs follow different developmental schedules that reflect different and rapidly changing functional needs.

Allometric tendencies are functionally justified shifts in proportions in ontogenetic and physiological processes (Dinnendahl and Kramer, 1957).

Typically, the equation $y = ax^b$ is used to examine allometric relations between body parts but it is of limited application in studies such as this. For example, this equation was applied to a variety of long bone parameters in California gulls but was found useful only for juveniles that had not yet reached full size (Carrier and Leon, 1990). We avoided this limitation by using an alternate allometric model based on growth models.

Sixty-five percent of our sample juveniles were C chicks, possibly because specimens were obtained by natural attrition and C chicks are smaller and least likely to survive (Parsons, 1975; Salzer and Larkin, 1990). Our results suggest that our sample may be biased toward smaller A/B chicks which, like C chicks, also may exhibit lower survival rates. Alternately, the appendicular bones of C chicks may grow at similar rates and proportions to those of A/B chicks, with weight differences due primarily to differences in soft tissue growth. Neither hypothesis can be ruled out with our data.

In summary, each of the 12 bone dimensions was best modeled by the Janoschek or Holling III models, in either their original or modified forms. We wish, however, to state two caveats. First, our sample includes bones from different birds at each age level, making this a cross-sectional rather than longitudinal study. Cross-sectional studies are limited by the fact that they tell us nothing about individual rates of growth, but only provide estimates of mean rates of growth for a population. Conducting a longitudinal study on bone growth in living wild gulls would be possible only with imaging technologies unavailable in the field. Second, our analysis focuses on changes in long-bone lengths and diameters, although considerable ontogenetic reshaping of bones in relation to function also occurs, a topic to be addressed in a future article.

ACKNOWLEDGMENTS

We thank U.S. Fish and Wildlife Service, for permission to collect skeletal specimens on Protection Island National Wildlife Refuge; Walla Walla College Marine Station for logistical support; Mark Johannson and Joey Maier for bone preparation; Joseph Galusha and Chrystal Spore for field assistance; Brian Dennis for the UMVU estimator in Eq. 12; and two anonymous reviewers for helpful suggestions.

LITERATURE CITED

- Burnham KP, Anderson DR. 2002. Model Selection and Multi-Model Inference: A Practical Information-Theoretic Approach, 2nd ed. New York: Springer. 488 p.
- Carrier D, Leon LR. 1990. Skeletal growth and function in the California gull (*Larus californicus*). *J Zool (London)* 222:375–389.
- Carrier DR, Auriemma J. 1992. A developmental constraint on the fledging time in birds. *Biol J Linn Soc* 47:61–77.

- Dennis B, Munholland PL, Scott JM. 1991. Estimation of growth and extinction parameters for endangered species. *Ecol Monogr* 61:115–143.
- Dinnendahl L, Kramer G. 1957. Über größenabhängige Änderungen von Körperproportionen bei Möwen (*Larus ridibundus*, *L. canus*, *L. argentatus*, *L. marinus*). *J Ornithol* 98:282–312.
- Dunn EH, Brisbin IL. 1980. Age-specific changes in the major body components and caloric values of herring gull chicks. *Condor* 82:398–401.
- Elowe KD, Payne S. 1979. Aging young herring gulls from measurements of body parts. *Bird Band* 50:49–55.
- Galilei G. 1638 [1914]. *Dialogues Concerning Two New Sciences*. New York: Macmillan. 328 p. Translated from the Italian and Latin into English by H. Crew and A. de Salvio.
- Gille U, Salomon FV. 1995. Bone growth in ducks through mathematical models with special reference to the Janoschek growth curve. *Growth Develop Aging* 59:207–214.
- Gille U, Salomon FV. 1999. Growth of duck bills. *Condor* 101:710–713.
- Gille U, Zachen F, Salomon FV. 2000. Brain, eye, and skull growth in embryonic geese. *Condor* 102:676–79.
- Gilliland SG, Ankney CD. 1992. Estimating age of young birds with a multivariate measure of body size. *Auk* 109:444–450.
- Gompertz B. 1825. On the nature of the function expressive of the law of human mortality, and a new mode of determining the value of live contingencies. *Philos Trans R Soc* 182:513–585.
- Hall R. 2000. A Mathematical Model for Longitudinal Bone Growth. Unpublished Master's Thesis, Corpus Christi College, University of Oxford. 33 p.
- Hayward JL, Verbeek NA. 2008. Glaucous-winged Gull (*Larus glaucescens*). In: Poole A, editor. *Birds of North America Online*. Ithaca, NY: Cornell Laboratory of Ornithology. Retrieved from <http://bna.birds.cornell.edu/species/059>.
- Henson SM, Dennis B, Hayward JL, Cushing JM, Galusha JG. 2007. Predicting the dynamics of animal behavior in field populations. *Anim Behav* 74:103–110.
- Holling CS. 1959. Some characteristics of simple types of predation and parasitism. *Can Entomol* 91:385–398.
- James-Veitch E, Booth ES. 1954. *Behavior and Life History of the Glaucous-Winged Gull*. Walla Walla College Publications of the Department of Biological Sciences and Biological Station, No. 12.
- Janoschek A. 1957. Das reaktionskinetische Grundgesetz und seine Beziehungen zum Wachstums- und Ertragsgesetz. *Stat Vjschr* 10:25–37.
- Klíma M. 1965. Evaluation of the so-called skeleton sum method, employed in investigations of growth allometry in birds. *Z Morphol Okolog Tiere* 55:250–258.
- Livezey BC, Storer RW. 1992. Morphometric comparison of skeletons of the western grebe complex *Aechmophorus* of the United States and Canada. *Condor* 94:668–679.
- Meunier K. 1959. Die Allometrie des Vogelflugels. *Z Wiss Zool* 161:444–482.
- Montes L, de Margerie E, Castanet J, de Ricqlès A, Cubo J. 2005. Relationship between bone growth rate and the thickness of calcified cartilage in the long bones of the Galloanseræ (Aves). *J Anat* 206:445–452.
- Olsson DM, Nelson LS. 1975. The Nelder-Mead simplex procedure for function minimization. *Technometrics* 17:45–51.
- Parsons J. 1975. Asynchronous hatching and chick mortality in the herring gull, *Larus argentatus*. *Condor* 78:481–492.
- Peek JM, Dennis B, Hershey T. 2002. Predicting population trends of mule deer. *J Wildlife Manage* 66:729–736.
- Press WH, Flannery BP, Teukolsky SA, Vetterling WT. 1986. *Numerical Recipes: The Art of Scientific Computing*. Cambridge: Cambridge University Press. 848 p.
- Price JS, Oyajobi BO, Russell RGG. 1994. The cell biology of bone growth. *Eur J Clin Nutr* 48:S131–S149.
- Salzer DW, Larkin GJ. 1990. Impact of courtship feeding on clutch and third-egg size in glaucous-winged gulls. *Anim Behav* 39:1149–1162.
- Shimizu K, Iwase K. 1981. Uniformly minimum variance unbiased estimation in lognormal and related distributions. *Commun Stat A Theory and Methods* 10:1127–1147.
- Schultz ZM. 1951. Growth in the glaucous-winged gull. Part 1. *Murrelet* 32:35–42.
- Schultz ZM. 1986. *On the Wings of the Wild Wind*, Occas Pap #21. Bellingham, WA: Center for Pacific Northwest Studies.
- Smith JE, Diem KL. 1972. Growth and development of young California gulls (*Larus californicus*). *Condor* 74:462–470.
- Vermeer K. 1963. The breeding ecology of the glaucous-winged gull (*Larus glaucescens*). Occas Pap BC Prov Mus, No. 13.